Dynamical effects of the four-wave mixing enhancement induced by constructive quantum interference*

Xue Yan(薛 艳), Wang Gang(王 刚), Wu Jin-Hui(吴金辉), Zhang Bing(张 冰), and Gao Jin-Yue(高锦岳)†

College of Physics, Jilin University, Changchun 130023, *China*
Key Lab of CLAMS of Educational Ministry, Changchun 130023, *China*

(Received 17 April 2010; revised manuscript received 20 June 2010)

In a four-level system of ultracold ^{87}Rb atoms, through analytical and numerical calculations we propose an efficient scheme to achieve the enhanced four-wave mixing process and demonstrate its dynamical control by various parameters such as the travel distance z, probe detuning δ and the probe pulse width τ. In particular, we find that the maximal intensity of the nonlinearly generated signal pulse can be about 80% of the initial input probe under the optimal condition. This greatly enhanced conversion efficiency occurs due to the constructive quantum interference between two different components of the generated signal pulse.

Keywords: four-wave mixing, quantum interference

PACS: 34.80.Pa, 42.50.–p, 42.65.–K **DOI:** 10.1088/1674-1056/20/3/033403

1. Introduction

The magnitude of conversion efficiency is always a problem in nonlinear frequency conversion processes.[1−4] Its value is relatively poor due to the extremely small higher-order nonlinear susceptibilities. Therfore, improving the higher-order nonlinear susceptibilities has become the key to achieving very high conversion efficiencies at desired frequencies. In traditional nonlinear optics, researchers pay more attention to the study of different optical crystals and focus on how to prepare crystals with large higher-order nonlinear susceptibilities.

With the recent development of quantum optics, a new method based on quantum interference has been proposed to improve the higher-order nonlinear susceptibilities. Using quantum interference, the absorption and dispersion properties in various media, such as atomic clouds or vapours, crystals doped with impurities and quantum well structures, can be well manipulated to inhibit the lower-order susceptibilities, which then allows a certain higher-order susceptibility to become dominant. In this field, there have been many theoretical and experimental investigations aimed at enhancing the higher-order susceptibilities as well as optimizing frequency conversion efficiencies in nonlinear optical processes.[4−11] For example, Harris *et al.*[10] found that it was theoretically possible to improve the third-order susceptibility on atomic resonance accompanied with little absorption. Jain *et al.*[6] experimentally observed that the four-wave-mixing (FWM) phenomenon was greatly enhanced by quantum interference in collisionally broadened Pb vapour. Most of these previous studies featured the double-lambda system,[8,11−15] in which atomic coherence is prepared between two long-lived stable or meta-stable states. One advantage of this system is that the stable (ground) and meta-stable states are immune to spontaneous decay so that the prepared atomic coherence is almost constant during a period limited by the excited state lifetimes. It is now well known that a negative atomic coherence with large absolute values is necessary and crucial for improving frequency conversion efficiency. One can use the adiabatic following technique[16−18] or the fractional stimulated Raman adiabatic process (STIRAP)[19−21] to optimize atomic coherence in the double-lambda system.

Apart from the double-lambda system, the so-called diamond system, which has four levels interacting with fields in a closed-loop configuration, is also a good candidate for achieving a highly efficient four-wave mixing processes via quantum coherence. Morigi *et al.*[22] has studied the phase-dependent proper-

*Project supported by National Natural Science Foundation of China (Grant Nos. 10774059 and 10904047), the National Basic Research Program of China (Grant No. 2006CB921103), the doctoral program foundation of institution of High Education of China (Grant No. 20060183046) and the basic research foundation of Jilin University of China (Grant No. 200903326).

†Corresponding author. E-mail: jygao@mail.jlu.edu.cn

© 2011 Chinese Physical Society and IOP Publishing Ltd

ties of population distribution in the diamond system and compared their results with those of the double-lambda system. Furthermore, Zibrov *et al.*[23] demonstrated the FWM process in a diamond system driven by two microwave fields and a cw optical field. Their study proved that atomic coherence prepared by microwave fields can be applied to improve nonlinear conversion efficiencies without the use of the fractional STIRAP or the adiabatic following technique, which are necessary for FWM but difficult in operation in the double-lambda system.

In this paper, without consideration of the fractional STIRAP or adiabatic following techniques, we discuss the coherently enhanced FWM process in a diamond system relevant to ultracold ^{87}Rb atoms (as shown in Fig.1). This diamond system is quite different from that in Ref. [23] because it is driven by three optical fields, i.e. two cw coupling fields Ω_1 and Ω_2 and a weak probe pulse Ω_3.

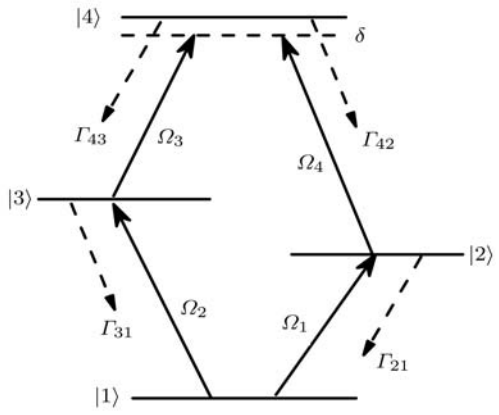


Fig. 1. Energy level diagram for a lifetime-broadened four-level ^{87}Rb cold atomic system where, in the presence of two strong continuous lasers Ω_1 and Ω_2, a weak probe pulse laser Ω_3 is fired to generate the signal field Ω_4.

Although the absolute value (25%) for optimized atomic coherence between intermediate levels is smaller than that (50%) between the lower levels in the double-lambda system, our diamond system has three specific advantages for achieving highly efficient FWM. First, it is much easier to obtain optimized atomic coherence with cw laser fields than with pulsed laser fields as far as the experiment is concerned. Second, there is no strict limit in the time duration of the weak probe pulse because the V subsystem composed of the three lower levels can quickly evolve into a steady state with invariable atomic coherence. More importantly, our numerical calculations show that the dynamically tunable FWM signal could be close to 80% in intensity of the initial input probe pulse due to the constructive quantum interference between two different components of the signal pulse.

2. The model equations and analytical solutions

Let us consider a lifetime broadened four-level system in the diamond configuration of ultracold ^{87}Rb atoms with a density of 10^{11} cm^{-3}, as shown in Fig. 1. In this system, the ground level $|1\rangle$ and the three excited levels $|2\rangle$, $|3\rangle$, $|4\rangle$ correspond to states $5^2S_{1/2}$, $5^2P_{1/2}$, $5^2P_{3/2}$ and $6^2S_{1/2}$, respectively. One remarkable disadvantage of the diamond system is the large spontaneous decay rates of the two intermediate levels, which will limit the attainable maximal value of atomic coherence and may reduce it significantly in the dynamical process. To avoid this negative effect, we choose two strong cw laser fields to drive the two lower dipole-allowed transitions so that atomic coherence with a large invariable absolute value can be established between the two intermediate levels. When the V subsystem composed of the three lower levels goes into its steady state, a weak probe pulse with a Gaussian profile $\Omega_3(z,t) = \Omega_{30}\exp[-((t-t_0-z/c)/\tau)^2]$ is sent into the medium to couple levels $|3\rangle$ and $|4\rangle$ so that a FWM signal can be generated. Here, Ω_{30} is the peak value of the initial probe Rabi frequency, τ is the time duration of the probe pulse and t_0 should be larger than the time necessary for the V subsystem to evolve into its steady state. $\Gamma_{21} = 36.1$ MHz, $\Gamma_{31} = 38.1$ MHz, $\Gamma_{42} = 14.48$ MHz and $\Gamma_{43} = 7.46$ MHz, respectively, represent the corresponding spontaneous decay rates and δ is the probe detuning.

In the interaction picture, with rotating-wave and electric-dipole approximations, the Hamiltonian reads as ($\hbar = 1$)

$$\begin{aligned} H_{\rm I}(z,t) = & -\Omega_1|2\rangle\langle 1| - \Omega_2|3\rangle\langle 1| - \Omega_3(z,t)|4\rangle\langle 3| \\ & - \Omega_4(z,t)|4\rangle\langle 2| + \text{H.C.} \end{aligned} \tag{1}$$

and the dynamical evolution for the density operator $\rho(z,t)$ of an atom located at z can be described by the well-known Liouville equation $\mathrm{i}\partial\rho/\partial t = [H_{\rm I},\rho] - \mathrm{i}(1/2)\{\Gamma,\rho\}$. In the following, we assume that the relative phases of all three applied fields are zero. The correct description of light pulse propagation in the atomic medium requires the Maxwell wave equations, namely

$$\frac{\partial\Omega_3}{\partial z} + \frac{1}{c}\frac{\partial\Omega_3}{\partial t} = \mathrm{i}k_{34}\rho_{43},$$

$$\frac{\partial \Omega_4}{\partial z} + \frac{1}{c}\frac{\partial \Omega_4}{\partial t} = \mathrm{i}k_{24}\rho_{42}, \quad (2)$$

which should be solved together with the set of equations for the density matrix elements ρ_{ij}. Here, $k_{34} = Nd_3^2\omega_3/\epsilon_0 c$ and $k_{24} = Nd_4^2\omega_4/\epsilon_0 c$ with N being the atomic density, ϵ_0 the permittivity of the vacuum, c the speed of light in vacuum and d_i the corresponding dipole moment of the transition driven by the i-th pulse laser Ω_i.

In the following, we will treat the whole coherent FWM process in two separate steps with the consideration that both cw fields are much stronger than the probe pulse: first, to prepare atomic coherence between the two intermediate levels with the cw coupling fields Ω_1 and Ω_2; second, to generate the FWM signal Ω_4 through stimulated Raman scattering of the probe pulse Ω_3. In Fig. 2, we plot the atomic coherence ρ_{23} in the V subsystem using exact numerical calculations based on the coupled Maxwell–Liouville equations. We can see that atomic coherence remains almost constant when the probe pulse is input with a suitable time delay, which means that the weak probe has little effect on the V subsystem and the two-step treatment is appropriate for our present purpose.

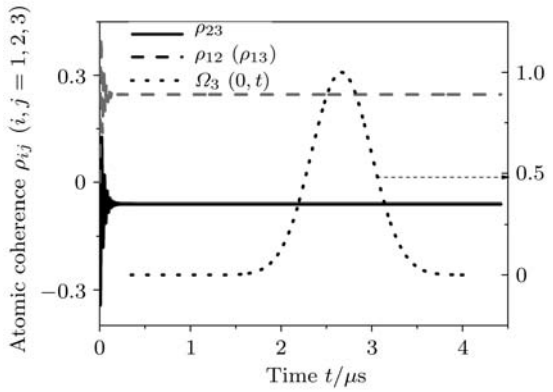


Fig. 2. The atomic coherence (corresponding to the left axis) vs the time t when the probe field (corresponding to the right axis) is input at the time of $5/\Gamma_{43}$ with travelling distance $z = 0.5$ cm; the parameters are: $\delta = 0$, $N = 5 \times 10^{11}$ cm^{-3}, $\Omega = 10\Gamma_{43}$, $\Omega_p = 0.1\Gamma_{43}$.

Now let us start the two-step discussion for FWM in the diamond system. Because Γ_{21} and Γ_{31} have almost the same values, we can set $\Omega_1 = \Omega_2 = \Omega$ to obtain the optimized atomic coherence. In this case, the relevant density matrix elements for the V subsystem are derived in the steady state as:

$$\rho_{12} = \rho_{13} = -\frac{\mathrm{i}\gamma\Omega}{4\Omega^2 + \gamma^2},$$
$$\rho_{22} = \rho_{33} = \rho_{23} = \frac{\Omega^2}{4\Omega^2 + \gamma^2}. \quad (3)$$

Once the V subsystem has come into the steady state described by Eq. (3), we can go to the second step, i.e., to apply the probe pulse to generate the FWM signal. Here we note that the probe should be weak enough to guarantee an unchanged population distribution and atomic coherence in the V subsystem (see Fig. 2). In this case, we can obtain from Eq. (3) the probability amplitudes of the three lower levels a_1, a_2, and a_3 with $\rho_{ij} = a_i a_j^*$, and further obtain a_4 by solving the simple Schrödinger equation (instead of the complicated Liouville equation). The latter owes to the fact that, in the weak probe limit, little population can be pumped to level $|4\rangle$ and a_1, a_2, and a_3 remains almost constant in the FWM process. Then it is the simple matter of deriving the following differential equation

$$\mathrm{i}\frac{\partial}{\partial t}a_4 = \delta a_4 - \Omega_3 a_3 - \Omega_4 a_2 - \mathrm{i}(\Gamma_{42} + \Gamma_{43})a_4, \quad (4)$$

whose solution for a_4 can be used to determine ρ_{43} and ρ_{42} together with the constant a_2 and a_3.

To attain an analytical solution of Ω_3 and Ω_4, we first perform the Fourier transform on both sides of Eqs. (2) and (4) with respect to time by defining $A(z,\omega)$, $M(z,\omega)$, and $S(z,\omega)$ as the Fourier transform of $a_4(z,t)$, $\Omega_3(z,t)$, and $\Omega_4(z,t)$, respectively. After combining the results and solving the corresponding differential equations (similar to the method used in Ref. [14]) with the initial condition that $M(0,\omega)$ is the Fourier transformation of $\Omega_3(0,t)$ at the entrance of the medium, we have:

$$S(z,\omega) = \frac{\mathrm{i}M(0,\omega)t_2}{\Lambda}\exp(\mathrm{i}Dz)\sin(\Lambda z)$$
$$M(z,\omega) = \frac{M(0,\omega)}{\Lambda}\exp(\mathrm{i}Dz) \times \left[\frac{-(k_2 - k_3)}{2}\sin(\Lambda z) + \Lambda\cos(\Lambda z)\right], \quad (5)$$

where

$$D = \frac{k_2 + k_3}{2}, \quad \Lambda = \left[\left(\frac{k_2 + k_3}{2}\right)^2 + t_2 t_3\right]^{1/2},$$
$$k_2 = \frac{k_{24}\rho_{22}}{\delta + \omega - 2\mathrm{i}\,(\gamma_2 + \gamma_3)} - \frac{\omega}{c},$$
$$k_3 = \frac{k_{34}\rho_{33}}{\delta + \omega - 2\mathrm{i}\,(\gamma_2 + \gamma_3)} - \frac{\omega}{c},$$
$$t_2 = \frac{k_{24}\rho_{32}}{\delta + \omega - 2\mathrm{i}\,(\gamma_2 + \gamma_3)}$$

and

$$t_3 = \frac{k_{34}\rho_{23}}{\delta + \omega - 2\mathrm{i}\,(\gamma_2 + \gamma_3)}.$$

Next we perform the inverse Fourier transform with respect to frequency ω for Eq. (5) to obtain the following results:

$$\Omega_3(z,t) = \frac{\Omega_3(0,0)}{4\sqrt{\pi}} \int \mathrm{d}\eta \Bigg(\exp\left[-\frac{\eta^2}{4} + \frac{\mathrm{i}\eta(t-t_0)}{\tau}\right] \times \left\{ \left(1 - \frac{k_2-k_3}{2\Lambda}\right) \exp[\mathrm{i}(D+\Lambda)z] \right\} + \left\{ \left(1 + \frac{k_2-k_3}{2\Lambda}\right) \exp[\mathrm{i}(D-\Lambda)z] \right\} \Bigg),$$

$$\Omega_4(z,t) = \frac{k_{24}\rho_{32}\Omega_3(0,0)}{2\sqrt{\pi}k_{24}\rho_{22} + k_{34}\rho_{33}} \int \mathrm{d}\eta \Bigg(\{\exp[\mathrm{i}(D+\Lambda)z] - \exp[\mathrm{i}(D-\Lambda)z]\} \exp\left[-\frac{\eta^2}{4} + \frac{\mathrm{i}\eta(t-t_0)}{\tau}\right] \Bigg). \quad (6)$$

In the following, we further simplify Eqs. (6) respectively in two different cases, e.g. the large probe detuning case $\delta \gg 0$ and the small probe detuning case $\delta \approx 0$. For a case with large enough probe detuning δ satisfying $(1+\omega/(\delta - 2\mathrm{i}(\Gamma_{42}+\Gamma_{43})))^{-1} \approx 1 - \omega/(\delta - 2\mathrm{i}(\Gamma_{42}+\Gamma_{43}))$, the following results can be derived:

$$\Omega_3(z,t) = \frac{k_{24}\rho_{22}}{k_{34}\rho_{33}+k_{24}\rho_{22}} \left[\Omega_3\left(0, t - \frac{z}{c}\right) + \frac{k_{34}\rho_{33}}{2k_{24}\rho_{22}} \exp(\mathrm{i}pz) \Omega_3\left(0, t - \frac{z}{v_g}\right) \right],$$

$$\Omega_4(z,t) = \frac{-k_{24}\rho_{32}}{k_{34}\rho_{33}+k_{24}\rho_{22}} \left[\Omega_3\left(0, t - \frac{z}{c}\right) - \exp(\mathrm{i}pz) \Omega_3\left(0, t - \frac{z}{v_g}\right) \right], \quad (7)$$

where

$$\frac{1}{v_g} = \frac{1}{c} + \frac{p}{\delta - 2\mathrm{i}(\Gamma_{42}+\Gamma_{43})}$$

and

$$p = p_1 + \mathrm{i}p_2 = \frac{k_{34}\rho_{33}+k_{24}\rho_{22}}{\delta - 2\mathrm{i}(\Gamma_{42}+\Gamma_{43})}.$$

Here p_1 represents the real part of p and p_2 is its imaginary part. For a case with small probe detuning δ satisfying $|\exp(\mathrm{i}pz)| \ll 1$, however, Eqs. (6) are simplified to:

$$\Omega_3(z,t) = \frac{k_{24}\rho_{22}}{k_{34}\rho_{33}+k_{24}\rho_{22}} \Omega_3\left(0, t - \frac{z}{c}\right),$$

$$\Omega_4(z,t) = \frac{-k_{24}\rho_{32}}{k_{34}\rho_{33}+k_{24}\rho_{22}} \Omega_3\left(0, t - \frac{z}{c}\right). \quad (8)$$

Until now we have obtained analytical solutions for the probe and signal pulses Ω_3 and Ω_4 propagating through a coherently prepared atomic medium in two different cases. What should be stressed is that the purpose for deriving Eqs. (7) and (8) is just to gain some physical insights into the coherent FWM process, and all the numerical calculations shown are based on the coupled Maxwell–Liouville equations. Fortunately, these exact numerical calculations are in good agreement with our approximate analytical solutions. In the next section, we will set $\Omega_4(z,t) = \Omega_{30} f(z,t)$ and $\Omega_3(z,t) = \Omega_{30} g(z,t)$ for convenience in analysis.

3. Discussions

In this section, as predicted by Eqs. (7) and (8), we discuss the coherent generation of the nonlinear signal pulse Ω_4 in two different cases: $\delta \gg 0$ and $\delta \approx 0$. From Eq. (8) we can see that, in the case of $\delta \approx 0$, both the generated signal pulse $\Omega_4(z,t)$ and the propagating probe pulse $\Omega_3(z,t)$ have the same group velocity c and the same Gaussian profile as the initial probe pulse $\Omega_3(0,t)$, but their magnitudes strongly depend on the atomic density, relevant dipole moments, as well as population distribution and atomic coherence related to the intermediate levels $|2\rangle$ and $|3\rangle$. In Fig. 3, we show the relevant exact numerical calculations, which confirm our above analytical results. It is clear that the signal is first generated and then enhanced during its propagation and there is no distortion of its Gaussian profile.

Equation (7) shows that, in the case of large probe detuning $\delta \gg 0$, the probe pulse $\Omega_3(z,t)$ will break into two components with the same time duration but different group velocities and amplitudes as it propagates in the coherently prepared medium. There are constructive or destructive quantum interferences between the two components, which occur alternatively with the travelling distance z. The same conclusions hold true for the generated signal pulse, while constructive interference between the signal components is always accompanied by destructive interference between the probe components and vice versa. Thus the nonlinear frequency conversion can be either from $\Omega_3(z,t)$ to $\Omega_4(z,t)$ or from $\Omega_4(z,t)$ to $\Omega_3(z,t)$ and the key is just the sign of $\exp(\mathrm{i}pz)$. Here the former corresponds to the generation and amplification of the signal pulse $\Omega_4(z,t)$ while the later corresponds to its depletion, and they oscillate periodically with the travelling distance z as shown in Fig. 4.

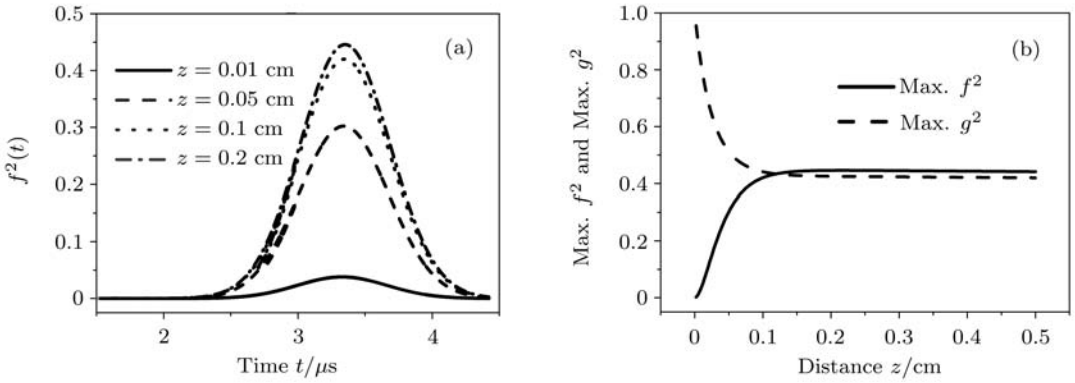


Fig. 3. (a) The $f^2(t)$ vs the time t for different travelling distance z; (b)the maximum values of $f^2(t)$ and the $g^2(t)$ at a specific time as functions of the travelling distance z. The parameters are the same as in Fig. 2.

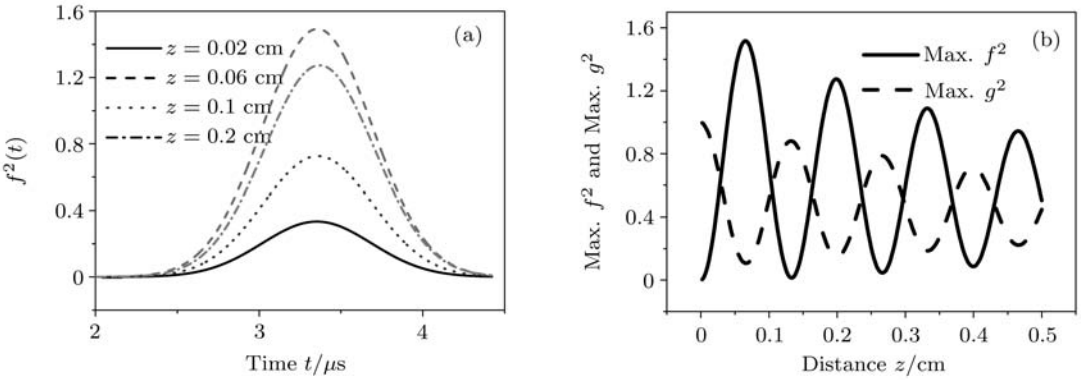


Fig. 4. (a) The $f^2(t)$ vs the time t for different travelling distance z; (b) the maximum values of $f^2(t)$ and $g^2(t)$ at a specific time as functions of the travelling distance z. $\delta = 38\Gamma_{43}$. Other parameters are the same as those in Fig. 2.

Moreover, one should note three points demonstrated in Fig. 4. First, magnitude oscillations of the signal and probe pulses gradually decrease when the travelling distance becomes longer and longer, which implies that these oscillations are damped. Comparing Eq. (7) with Eq. (8), we can see that the oscillations will finally achieve tranquilization with field amplitudes similar to those in the small probe detuning case if the sampling length is long enough. Second, during the first few oscillation periods, at certain traveling distances, the squared magnitude of the signal pulse can be larger than that of the input probe pulse at the initial time. In our calculation, the maximal value of $f^2(t)$ is close to 160%, which implies that, according to the definitions of Rabi frequency $\Omega = \mu E/2\hbar$ and dipole moment $\mu = (2\Gamma\hbar\varepsilon_0\lambda^3/8\pi^2)^{1/2}$, the generated signal pulse is about 80% in intensity of the initial input probe pulse. Finally, we would like to point out that there exists no pulse distortion either in the small probe detuning case or in the large probe detuning case [see Figs. 3(a) and 4(a)].

The above discussions clearly show that not only traveling distance but also probe detuning plays an important role in improving coherent FWM efficiency. To better understand the effect of the probe detuning δ, we further plot in Fig. 5 the maximal value of $f^2(t)$ vs. δ at a certain traveling distance $z = 0.5$ cm. We can see that there exist two critical probe detuning points with the same absolute value δ_0, around which the diamond system has quite different dynamical responses. When $|\delta| < \delta_0$, the signal magnitude remains almost constant and is relatively small, while in the opposite case it oscillates with the probe detuning and can become much larger. Here, the oscillation behavior of $f^2(t)$ stems from the alternatively occurring constructive and destructive quantum interference between the two components of the signal pulse. With the increase of δ, the difference between group velocities of these two components becomes smaller and smaller, which then leads to better quantum interference, so that much stronger signals can be generated. From Eq. (7), we can see that the oscillation period of $f^2(t)$ is determined by p_1 and becomes larger and larger with the increase of δ. We further note that

the maximum and minimum of $f^2(t)$ correspond to $p_1 = (2n+1)\pi/z$ and $p_1 = 2n\pi/z$, $n = 0, 1, 2, \ldots$, respectively.

It is well known that atomic coherence established by the fractional STIRAP technique in the double-lambda system has a Gaussian profile in time, which greatly limits time durations of the input probe and the generated signal. In our diamond system, however, when the subsystem consisting of the three lower levels goes into its steady state after a damped oscillation, atomic coherence remains almost constant so that the probe and signal pulses could have rather long time durations without any limitation. This fact allows us to plot, in Fig. 6, the maximal value of $f^2(t)$ vs. the probe time duration, where the signal magnitude first increases dramatically and then quickly reaches a steady value when the probe time duration becomes long enough. Thus we can choose a probe pulse with suitable time durations to attain large conversion efficiencies in the coherent FWM process.

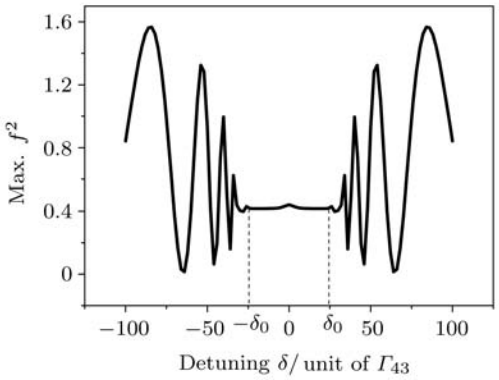


Fig. 5. The maximum value of $f^2(t)$ as a function of the probe detuning δ with parameter $z = 0.5$ cm. Other parameters are the same as those in Fig. 2.

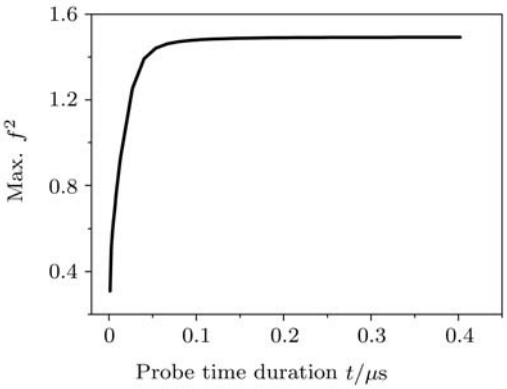


Fig. 6. The maximum value of $f^2(t)$ as a function of the time duration of the probe pulse. $z = 0.5$ cm. Other parameters are the same as those in Fig. 4.

4. Concluding remarks

In summary, we have shown that coherent enhancement of the FWM process can be achieved in a lifetime broadened four-level atomic system in the diamond configuration, where the coherent preparation preceding the nonlinear mixing requires two strong cs laser fields. By varying the traveling distance z, the probe detuning δ and the probe time duration τ, one can easily control the FWM process to achieve high frequency conversion efficiencies from the input probe to the generated signal. In particular, when the probe detuning δ is large enough, at a proper traveling distance z, the generated signal can be close to 80% in intensity of the initial input probe pulse having a suitable time duration. This fact implies a frequency conversion efficiency much larger than those obtained by the fractional STIRAP technique[14,21] and those obtained by resonant four-wave mixing in the ultra-slow propagation regime.[24] Although realistic parameters of ultracold ^{87}Rb atoms have been used in calculation, our proposed scheme for coherently enhanced FWM may be employed for efficient IR[25] or UV[26] generation when a different manifold of atomic levels is used.

References

[1] Ham B S, Shahriar M S and Hemmer P R 1999 *Opt. Lett.* **24** 86

[2] Wu Y, Saldana J and Zhu Y F 2003 *Phys. Rev.* A **67** 013811

[3] Fu P M, Jiang Q, Liu X, Mi X, Sun J, Wu L A,Yu Z H and Zuo Z C 2007 *Chin. Phys.* **16** 1042

[4] Hakuta K, Marmet L and Stoicheff B P 1991 *Phys. Rev. Lett.* **66** 596

[5] Gong S Q, Niu Y P and Sun H 2007 *Chin. Phys.* **16** 429

[6] Jain M, Yin G Y, Field J E and Harris S E 1993 *Opt. Lett.* **18** 998

[7] Petch J C, Keitel C H, Knight P L and Marangos J P 1996 *Phys. Rev.* A **53** 543

[8] Merriam A J, Sharpe S J, Xia H, Manuszak D, Yin G Y and Harris S E 1999 *Opt. Lett.* **24** 625

[9] Dorman C, Kucukkara I and Marangos J P 1999 *Phys. Rev.* A **61** 013802
[10] Harris S E, Field J E and Imamoglu A 1990 *Phys. Rev. Lett.* **64** 1107
[11] Jain M, Xia H, Yin G Y, Merriam A J and Harris S E 1996 *Phys. Rev. Lett.* **77** 4326
[12] Johnsson M T and Fleischhauer M 2002 *Phys. Rev.* A **66** 043808
[13] Payne M G and Deng L 2002 *Phys. Rev.* A **65** 063806
[14] Deng L, Payne M G and Garrett W R 2001 *Phys. Rev.* A **63** 043811
[15] Payne M G and Deng L 2003 *Phys. Rev. Lett.* **91** 123602
[16] Crisp M D 1973 *Phys. Rev.* A **8** 2128
[17] Shakhmuratov R N and Odeurs J 2003 *Phys. Rev.* A **68** 043802
[18] Shakhmuratov R N, Odeurs J, Coussement R, Megret P, Kozyreff G and Mandel P 2001 *Phys. Rev. Lett.* **87** 153601
[19] Bergmann K, Theuer H and Shore B W 1998 *Rev. Mod. Phys.* **70** 1003
[20] Ye C Y, Sautenkov V A, Rostovtsev Y V and Scully M O 2003 *Opt. Lett.* **28** 2213
[21] Sautenkov V A, Ye C Y, Rostovtsev Y V, Welch G R and Scully M O 2004 *Phys. Rev.* A **70** 033406
[22] Morigi G, Franke-Arnold S and Oppo G 2002 *Phys. Rev.* A **66** 053409
[23] Zibrov A S, Matsko A B and Scully M O 2002 *Phys. Rev. Lett.* **89** 103601
[24] Kang H, Hernandez G and Zhu Y F 2004 *Phys. Rev.* A **70** 061804(R)
[25] Zheng D, Gordon L A, Wu Y S, Feigelson R S, Fejer M M and Byer R L 1998 *Opt. Lett.* **23** 1010
[26] Fry E S, Lukin M D, Walther T and Welch G R 2000 *Opt. Commun.* **179** 499